Low-lying dipole strength distribution in 204Pb

Shizuma, T.; Endo, S.; Kimura, A.; Massarczyk, R.; Schwengner, R.; Beyer, R.; Hensel, T.; Hoffmann, H.; Junghans, A.; Römer, K.; Turkat, S.; Wagner, A.; Tsoneva, N.;

Originally published:

October 2022

Physical Review C 106(2022), 044326

DOI: https://doi.org/10.1103/PhysRevC.106.044326

Low-lying dipole strength distribution in ^{204}Pb

T. Shizuma,[1] S. Endo,[2] A. Kimura,[2] R. Schwengner,[3] R. Beyer,[3] T. Hensel,[3]
H. Hoffmann,[3] A. Junghans,[3] T. Römer,[3] S. Turkat,[3], A. Wagner,[3] and N. Tsoneva[4]
[1]*National Institutes for Quantum Science and Technology, Tokai, Ibaraki 319-1106, Japan*
[2]*Japan Atomic Energy Agency, Tokai, Ibaraki 319-1195, Japan*
[3]*Helmholtz-Zentrum Dresden-Rossendorf, Dresden 01328, Germany*
[4]*Extreme Light Infrastructure (ELI-NP), Horia Hulubei National Institute for R&D in Physics and Nuclear Engineering (IFIN-HH),*

(Dated: May 10, 2022)

Dipole and quadrupole strength distribution of ^{204}Pb was investigated via a nuclear resonance fluorescence experiment using bremsstrahlung produced using an electron beam at a kinetic energy of 10.5 MeV at the linear accelerator ELBE. We identified 136 states resonantly excited at energies from 3.6 to 8.4 MeV. The present experimental results were used to investigate the $E1$ transition probabilities by comparison with predictions from the quasiparticle-phonon model (QPM) with the self-consistent energy-density functional (EDF).

PACS numbers: PACS number(s): 21.10.Hw, 23.20.-g, 25.20.Dc, 27.40.+z

I. INTRODUCTION

Low-lying electric dipole ($E1$) excitation in atomic nuclei has attracted considerable interest during the past decades, caused by significant progress in experimental and theoretical studies of its properties [1]. It has been observed as a local accumulation of the $E1$ strength near the particle threshold in both stable and unstable nuclei over a broad range of nuclei [2–11]. This structure is commonly denoted as the pygmy dipole resonance (PDR), because the $E1$ strength is weak relative to that of the giant dipole resonance (GDR) which exhausts almost all the $E1$ strength predicted by the Thomas-Reiche-Kuhn (TRK) sum rule [12].

The geometric picture of the PDR is an out-of-phase oscillation of excess neutrons against an almost isospin-saturated ($N \approx Z$) core [13–15]. Microscopically, the PDR is explained as a sequence of excited one-particle-one-hole excitations ($1p-1h$), which act coherently and therefore cause an increased transition strength [16, 17]. Since the PDR strength is correlated with the neutron skin thickness [18, 19] which is related to nuclear symmetry energy [20, 21] and the equation of state (EOS) of the neutron-rich matter [22], the investigation of the PDR may provide useful information on the properties of the neutron stars [23].

Another interesting aspect of low-energy excitations, and in particular of the PDR, is that they involve interactions resulting from binding of complex configurations and the GDR related to nuclear polarization effects. A quasi-particle-random-phase-approximation (QRPA), taking into account only coherence superpositions of two-quasiparticle excitations is not enough to explain in detail the structure of nuclear excited states in the PDR region. Rather, an expanded approach is needed which explicitly takes into account the interactions between multi-quasiparticle configurations.

Furthermore, recent studies of nuclear reactions of astrophysical interest show that the reaction cross-sections strongly depend on the low-energy part of the electromagnetic dipole strength function and the PDR [11, 24, 25]. Such enhancement can have a strong impact on nucleosynthesis of heavier elements in stellar environments [11, 25]. It is known that lead isotopes may play important role in the s-process of nucleosynthesis. From our previous studies in the semi-magic ^{206}Pb nucleus we found that the presence of a PDR mode can greatly affect the ^{205}Pb radiative neutron capture cross section, a reaction of relevance to the destruction of ^{205}Pb during the s-process [11].

The stable lead isotopes including ^{204}Pb are suitable for studying the PDR since they exhibit an appreciable amount of low-lying dipole strength [3, 11, 26]. So far, the low-lying dipole distribution below 6.75 MeV in ^{204}Pb has been measured in nuclear resonance fluorescence (NRF) experiments with bremsstrahlung [26]. In the present work, the information was extended up to the neutron separation energy of 8.395 MeV by using higher energy bremsstrahlung. The experimental results are compared with predictions from the self-consistent energy-density functional (EDF) theory and the three-phonon quasiparticle-phonon model (QPM) [14, 16, 17].

II. EXPERIMENTAL PROCEDURE

The present NRF measurement on ^{204}Pb was carried out at the bremsstrahlung facility γELBE [27] of the Helmholtz-Zentrum Dresden-Rossendorf (HZDR). Bremsstrahlung was produced using an electron beam at a kinetic energy of 10.5 MeV with an average beam current of 470(?) μA at a micropulse repetition rate of 13 MHz. The electron beam hit a radiator consisting of a niobium foil with a thickness of 5(?) μm. The electron energy was chosen as the flux was sufficiently high up to the neutron separation energy. The bremsstrahlung was collimated by an Al collimator with a length of 2.6 m and an opening angle of 5 mrad. A cylindrical Al

absorber with a length of 10 cm was placed between the radiator and the collimator to reduce the low-energy bremsstrahlung.

The target consisted of a metallic disk of ^{204}Pb with a diameter of 20 mm tilted by 45° about a vertical axis perpendicular to the beam. The target mass was 1.9 g, enriched to 99.94% in ^{204}Pb. The lead disk was combined with 300 mg of boron, enriched to 99.5% in ^{11}B, that was also shaped to a disk of 20 mm diameter to determine the photon flux from known scattering cross sections of levels in ^{11}B.

Scattered photons were measured with four high-purity germanium(HPGe) detectors with relative efficiencies of 100%. All HPGe detectors were surrounded by escape-suppression shields made of bismuth germanate(BGO) scintillation detectors. Two HPGe detectors were placed horizontally at 90° relative to the photon beam direction at a distance of 28(???) cm from the target. The other two HPGe detectors were placed vertically at 127° to the beam at a distance of 32(???) cm from the target. The ratios of the γ-ray intensities measured at 90° and 127° are used to distinguish between dipole and quadrupole radiation. To reduce the contribution of low-energy photons, absorbers of 8(???)-mm Pb plus 3(???)-mm Cu were placed in front of the detectors at 90°, and 3(???)-mm Pb plus 3(???)-mm Cu were used for the detectors at 127°. Spectra of scattered photons were measured for 126(???) hours. Part of a spectrum including events measured with the two detectors at 127° relative to the beam is shown in Fig. 1. Further details of the measurement techniques are given in Refs. [28, 29].

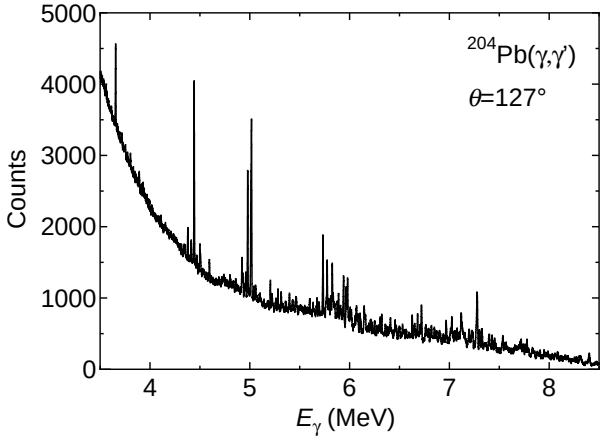

FIG. 1: Part of a spectrum of photons scattered from ^{204}Pb combined with ^{11}B, measured during the irradiation with bremsstrahlung produced by electrons at the kinetic energy of 10.5 MeV. This spectrum is the sum of the spectra measured with the two detectors at 127° relative to the beam.

III. RESULTS

In photon scattering experiments, the energy-integrated scattering cross section I_s of an excited state at the energy of E_x can be deduced from the measured intensity of the respective transitions to the ground state [30]. It can be determined relative to the known integrated scattering cross sections $I_s(E_x^{\rm B})$ of states in ^{11}B [31]:

$$\frac{I_s(E_x)}{I_s(E_x^{\rm B})} = \left(\frac{I_\gamma(E_\gamma,\theta)}{W(E_\gamma,\theta)\Phi_\gamma(E_x)N_N\lambda}\right) \times \left(\frac{I_\gamma(E_\gamma^{\rm B},\theta)}{W(E_\gamma^{\rm B},\theta)\Phi_\gamma(E_x^{\rm B})N_N^{\rm B}\lambda^{\rm B}}\right)^{-1}.$$

Here, $I_\gamma(E_\gamma,\theta)$ and $I_\gamma(E_\gamma^{\rm B},\theta)$ denote efficiency-corrected intensities of a ground-state transition at E_γ and of a ground state transition in ^{11}B at $E_\gamma^{\rm B}$, respectively, observed at a scattering angle θ to the beam. $W(E_\gamma,\theta)$ and $W(E_\gamma^{\rm B},\theta)$ represent the angular correlations of these transitions. The quantities $\Phi(E_x)$ and $\Phi_\gamma(E_x^{\rm B})$ are the photon fluxes at the energy of the considered level and at the energy of a level in ^{11}B, respectively. The quantities N_N and $N_N^{\rm B}$ stand for the numbers of nuclei in the ^{204}Pb and ^{11}B targets, respectively. The quantities λ and $\lambda^{\rm B}$ are the correction factors of atomic and self-absorption for the levels at E_x in ^{204}Pb and at $E_x^{\rm B}$ in ^{11}B, respectively. These correction factors were determined according to Eq.(19) in Ref. [32]. The determination of the integrated cross sections relative to the ones of states in ^{11}B has the advantage that the efficiencies of the detectors and the photon flux are needed in relative units only. We calculated the energy-dependent efficiencies for the four HPGe detectors by using GEANT4 [33]. The simulated efficiency curves were checked by using efficiencies measured with a ^{226}Ra calibration source. The bremsstrahlung spectrum was calculated by using a code [34] based on the approximation given in Ref. [35] and including a screening correction according to Ref. [36]. The calculated curve of the photon flux fits the experimental value derived from measured intensities, known integrated cross sections [31] and angular distributions [37] of transitions in ^{11}B.

The integrated scattering cross section I_s is related to the partial decay width Γ_0 to the ground state and the total decay width Γ according to

$$I_s = \int \sigma_{\gamma\gamma} dE = \frac{2J_x+1}{2J_0+1}\left(\frac{\pi\hbar c}{E_x}\right)^2 \frac{\Gamma_0^2}{\Gamma}, \qquad (1)$$

where $\sigma_{\gamma\gamma}$ is the elastic scattering cross section, J_0 and J_x denote the spins of the ground state and the excited state, respectively.

Spins of the excited states were deduced by comparing the ratios of γ-ray intensities measured with the HPGe detectors at two different angles with theoretical predications. The optimum combination is angles of 90° and 127° because the ratios for the respective spin sequences $0-1-0$ and $0-2-0$ differ most at these angles. The expected values are $W(90°)/W(127°)_{0-1-0} = 0.74$ and

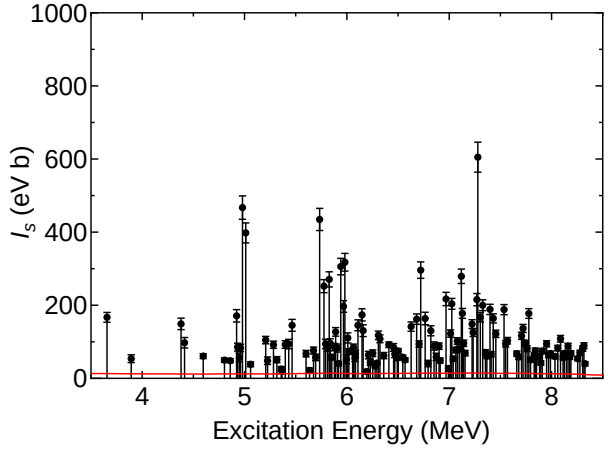

FIG. 2: Integrated scattering cross sections deduced from the present experiment. The detection limits for I_s are shown with a red line.

$W(90°)/W(127°)_{0-2-0} = 2.18$, taking into account the finite solid angle of the detectors.

The deduced values for excitation energies, angular distribution ratios, spin assignments, the ratios Γ_0^2/Γ, and branching ratios into the ground state are listed in Table I. Figure 2 shows the integrated cross sections deduced from the present experimental data. We observed 134 states with $J = 1$ and 2 states with $J = 2$ below the neutron separation energy, including 95 states newly identified in this work. A comparison of the Γ_0^2/Γ ratios obtained in the present experiment with previous work [26] is also shown in Table I. The present results are generally in good agreement with those previously published. Spins for 14 states known in previous work were newly determined. The present $J = 1$ spin assignment for the 3893-keV level is not consistent with the previous $J = 2$ assignment [26]. In addition, the resonance states at 5610 and 6420 keV reported previously [26] could not be confirmed.

The detection limit for a 95% confidence level is defined as $A_{DL} = 2.8\sqrt{2B}$ [38], where B is the integral over a background interval of full width at half maximum (FWHM) of a nearby peak, which has been applied in similar experiments [39, 40]. The detection limits converted to I_s is shown with a red line in Fig. 2. The state with the smallest I_s is the one at 6194 keV with 19(6) eV b. At this peak, we obtain $A_{\rm PEAK}/A_{\rm DL} = 1.4(4)$ from the 127° spectra. Toward high energy, the background decreases rapidly, while the background integral increases. For the highest peak given in Fig. 2 at 8327 keV, we obtain $A_{\rm PEAK}/A_{\rm DL} = 3.8(5)$.

The reduced electric dipole transition probabilities $B(E1)\uparrow$ can be extracted from Γ_0 using the following relationship:

$$B(E1)\uparrow = 2.865\frac{\Gamma_0}{E_\gamma^3}\ [10^{-3}e^2fm^2], \qquad (2)$$

where Γ_0 is given in units of meV and E_γ in units of MeV. From the present work, the total $E1$ strength of $\Sigma B(E1) = 0.613(6)$ e^{2}fm^2 below $E_x = 8.327$ MeV was obtained assuming $E1$ nature for the observed dipole transitions. If one would assume $M1$ strengths in ^{204}Pb comparable to ^{206}Pb [11] and ^{208}Pb [41], the results on the total $E1$ strength would change by at most 10%. Therefore, it would not affect the conclusion on the gross properties of the $E1$ strength distribution discussed below. The present total $E1$ strength corresponds to 0.546(6)% of the energy-weighted TRK sum rule value, which can be compared to the values of 0.79(1)% for ^{206}Pb [42], 0.35(2)% for ^{207}Pb [43], and 1.01(6)% for ^{208}Pb [41].

IV. DISCUSSION

A. Theoretical Model

Theoretical investigations of the spectral distributions of low-lying dipole excited states in the semi-magic ^{204}Pb nucleus and their relation to the PDR were conducted with the EDF theory and the three-phonon QPM [14, 16, 17]. An important advantage of the EDF+QPM approach is the description of the excited state wave functions in terms of QRPA phonons which are defined [44] by the equation:

$$Q^+_{\lambda\mu i} = \frac{1}{2}\sum_{jj'}\Big(\psi^{\lambda i}_{jj'}A^+_{\lambda\mu}(jj') - \varphi^{\lambda i}_{jj'}\widetilde{A}_{\lambda\mu}(jj')\Big), \qquad (3)$$

where $j \equiv (nljm\tau)$ is a single-particle proton or neutron state; $A^+_{\lambda\mu}$ and $\widetilde{A}_{\lambda\mu}$ are time-forward and time-backward operators, coupling two-quasiparticle ($2QP$) creation or annihilation operators to a total angular momentum λ with projection μ by means of the Clebsch-Gordan coefficients $C^{\lambda\mu}_{jmj'm'} = \langle jmj'm'|\lambda\mu\rangle$. The excitation energies of the phonons and the time-forward and time-backward amplitudes $\psi^{\lambda i}_{j_1j_2}$ and $\varphi^{\lambda i}_{j_1j_2}$ in Eq. (3) are determined by solving QRPA equations [44]. QRPA is also commonly called the "quasi-boson" approximation, as QRPA phonons are associated with pure bosonic states [45]. In the QPM the phonon operators satisfy commutation relations which take into account the internal fermionic structure of the phonons, thus satisfying the Pauli principle. Furthermore, the QRPA phonons are used as building blocks of the three-phonon QPM model configuration space [44, 46], which provides a microscopic way to multi-configurational mixing. For spherical even-even nuclei, the model Hamiltonian is diagonalized on an orthonormal set of wave functions constructed from one-, two-, and three-phonon configurations:

$$\Psi_\nu(JM) = \Bigg\{ \sum_i R_i(J\nu) Q^+_{JMi} + \sum_{\substack{\lambda_1 i_1 \\ \lambda_2 i_2}} P^{\lambda_1 i_1}_{\lambda_2 i_2}(J\nu) \left[Q^+_{\lambda_1\mu_1 i_1} \times Q^+_{\lambda_2\mu_2 i_2} \right]_{JM} \tag{4}$$

$$+ \sum_{\substack{\lambda_1 i_1 \lambda_2 i_2 \\ \lambda_3 i_3 I}} T^{\lambda_1 i_1 \lambda_2 i_2 I}_{\lambda_3 i_3}(J\nu) \left[\left[Q^+_{\lambda_1\mu_1 i_1} \otimes Q^+_{\lambda_2\mu_2 i_2} \right]_{IK} \otimes Q^+_{\lambda_3\mu_3 i_3} \right]_{JM} \Bigg\} \Psi_0$$

where R, P and T are unknown amplitudes, and ν labels the number of the excited states.

The nature of nuclear excitation can be studied by examining the spatial structure of the transition. This is achieved by analyzing the one-body transition densities, $\delta\rho(r)$, which are related to the non-diagonal elements of the one-body nuclear density matrix [16, 17]. By analyzing the transition density spatial pattern we obtain a very detailed picture, for example, of the radial distribution and localization of the excitation process. The electromagnetic transition matrix elements are calculated for transition operators including the interaction of quasiparticles and phonons [45] where exact commutation relations are implemented which is a necessary condition in order to satisfy the Pauli principle.

B. Comparison with the experimental results

Consistent with previous investigations of $E1$ strength in various nuclei [11, 16, 17, 47, 48], the present QPM calculations are performed with single-particle energies obtained in a self-consistent manner from EDF approach linked to fully self-consistent Hartree-Fock-Bogoliubov (HFB) calculations. The excited states are calculated with a residual interaction represented in separable form with strength parameters fixed empirically [17]. As a further advantage over other QRPA models, the QPM approach incorporates a multiphonon model space built of natural and unnatural parity states. Here, the model basis is constructed of one-, two-, and three-phonon (microscopically described) configurations with $J^\pi = 1^\pm$, 2^+, 3^-, 4^+, 5^-, 6^+ and 7^- and excitation energies E_x up to 9 MeV, in agreement with the range of the experimental data. Previous QRPA and QPM calculations of the $E1$ spectral distributions in ^{206}Pb and ^{208}Pb [11, 47] indicate enhanced $E1$ strength in the energy range below the neutron threshold with respect to the shape of a Lorentz-like strength function used to analyze the GDR. Theoretically and experimentally, it was found that the total $E1$ strength associated with the PDR increases with the increase in the isospin asymmetry of these nuclei defined by the N/Z ratio [11]. The detailed examination of proton and neutron transition densities of the individual QRPA 1^- states with predominantly neutron structure and located in the energy range $E_x \approx$ 6.5-7.5 MeV in ^{204}Pb, reveals the dominance of neutron-skin oscillations. They can be associated with a PDR mode which is shown in Fig.3 (top panel). The defining characteristic of the PDR neutron transition density is the nodal structure [16, 17]. In particular, the radial transition form factors correspond to a classical droplet wobbling mode in which matter is oscillating in radial direction as a standing compression surface wave. In quantum nuclear systems, the PDR skin modes correspond to a diffusivity oscillation, very different from the collective modes like the GDR shown in Fig.3 (bottom panel). The theoretical calculations of neutron and proton transition densities confirm the unique character of the low-lying 1^- states in ^{204}Pb. Theoretically, the description of the spectral distribution of the low-lying dipole strength and the fine structure of nuclear excitations requires to couple the 1^- one-phonon QRPA doorway states to more complex configurations which, in turn, are coupled again to other configurations. This coupling causes a fragmentation and a shift of the low-lying $E1$ strength toward lower energy which is achieved in a EDF+three-phonon QPM approach [17].

In Figs. 4(a) and 4(b), the experimental $B(E1)$ values are compared with the EDF+QPM calculations. The total measured $B(E1)$ value up to E_x=8.327 MeV amounts to $\Sigma B(E1)$=0.613(6) e^{2}fm^2. The corresponding QPM value above the experimental sensitivity limits is $\Sigma B(E1)$=0.971 e^{2}fm^2. Overall, the theoretical results in ^{204}Pb are in good agreement with the experiment, with respect to the low-lying $E1$ strength distribution pattern, the total $B(E1)$ strength, and with the TRK value. In particular, the obtained total $B(E1)$ strength located below $E_x \approx$8.4 MeV obtained by the experiment and the EDF+QPM approach exhausts approximately 0.6% and 1%, respectively. The QPM spectrum which is spread at excitation energy E_x larger than $\approx$7 MeV indicates larger $E1$ strength than the one experimentally observed. We point out that these differences are not a matter of the interaction parameters but originate in the quasiparticle spectrum which indicates a stronger coupling to low-energy GDR.

By comparing the QRPA to the multiphonon EDF+QPM calculations we find that the pure two-quasiparticles $E1$ QRPA strength below the neutron

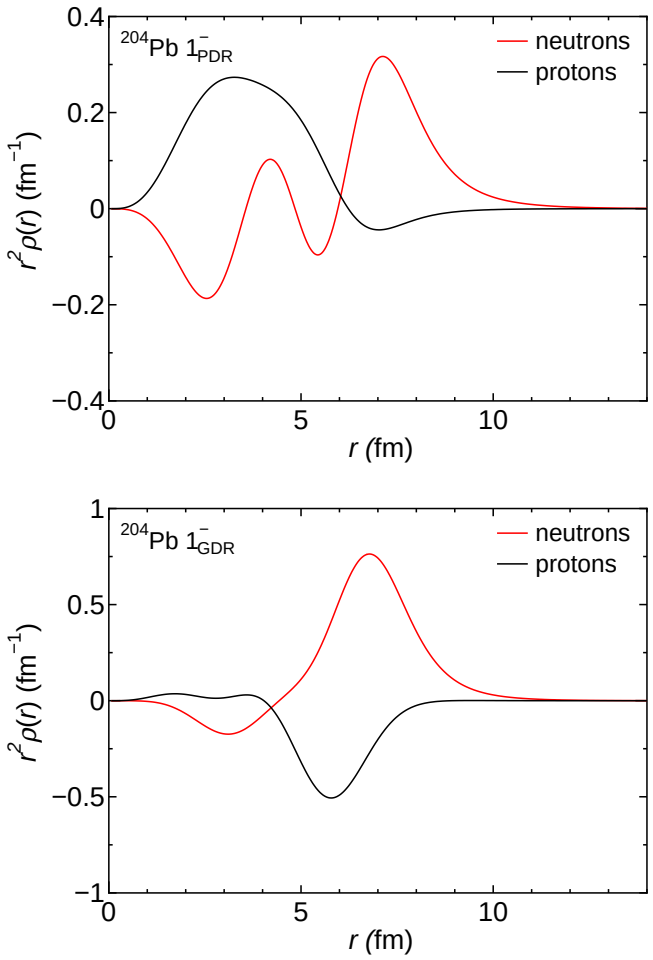

FIG. 3: (top) Summed neutron and proton transition densities of the $[1^-_{\rm PDR}]$ states and (bottom) the same for the $[1^-_{\rm GDR}]$ states obtained from QRPA calculations in ^{204}Pb.

threshold in ^{204}Pb is strongly fragmented over many 1^- excited states. Of particular interest are the QPM lowest-lying 1^-_1 at E_x(QPM)=3.566 MeV and 1^-_2 at E_x(QPM)=3.903 MeV states which are without QRPA counterpart because they contain a two-phonon quadrupole-octupole $[2^+_1 \otimes 3^-_1]$ configuration, which accounts for ≈50% of the 1^-_1 and ≈25% of the 1^-_2 QPM wave function, respectively. The theoretical $B(E1)\uparrow$ values of these 1^- states are: $B(E1, \text{g.s.} \rightarrow 1^-_1)_{\rm QPM} = 16 \times 10^{-3}$ e^{2}fm^2 and $B(E1, \text{g.s.} \rightarrow 1^-_2)_{\rm QPM} = 1.3 \times 10^{-3}$ e^{2}fm^2. The experimentally observed dipole states located at E_x = 3.656 and 3.892 MeV with $B(E1)\uparrow$= $11.3(9) \times 10^{-3}$ and $3.4(7) \times 10^{-3}$ e^{2}fm^2, respectively, may correspond to these predicted 1^- states.

V. SUMMARY

The dipole strength distribution in ^{204}Pb up to the neutron separation energy has been studied in a photon scattering experiment at the ELBE bremsstrahlung facility by using an electron beam at a kinetic energy of 10.5 MeV. We identified 134 $J = 1$ and 2 $J = 2$ resonantly excited states below 8.4 MeV. The experimental results were used to investigate the low-lying $E1$ strength and compared with predictions from the self-consistent energy-density functional (EDF) and the quasiparticle-phonon model (QPM). The EDF+QPM calculations reproduced the gross properties of the $E1$ strength observed below the neutron separation energy in ^{204}Pb. Analysis of the proton and neutron transition densities revealed that the low-lying $E1$ strength is mainly due to the neutron-skin oscillations. However, more complex configurations due to coupling of 1^- to multi-phonon states which causes a fragmentation and a shift of the low-lying $E1$ strength toward lower energy were also observed.

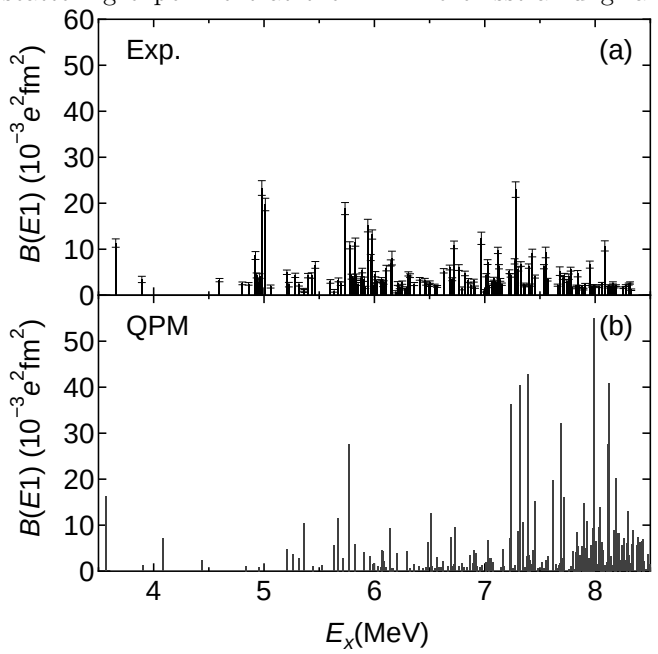

FIG. 4: $B(E1)\uparrow$ values deduced from the present NRF experiment (a) and the same for the EDF+QPM calculations (b) in ^{204}Pb.

Acknowledgments

We thank the staff of the ELBE accelerator facility for cooperation during the experiments and A. Hartmann for the technical assistance. This work was supported in part by Grants-in-Aid for Scientific Research(C)(20K04007) from the Japan Society for the Promotion of Science(JSPS). N. Tsoneva was supported by the Romanian Ministry of Research and Innovation under contract PN 19 06 01 05.

[1] D. Savran, T. Aumann, and A. Zilges, Prog. Part. Nucl. Phys. **70**, 210 (2013).

[2] A. Leistenschneider, T. Aumann, K. Boretzky, D. Cortina, J. Cub, U. Datta Pramanik, *et al.*, Phys. Rev. Lett. **86**, 5442 (2001).

[3] N. Ryezayeva, T. Hartmann, Y. Kalmykov, H. Lenske, P. von Neumann-Cosel, V. Yu. Ponomarev, *et al.*, Phys. Rev. Lett. **89**, 272502 (2002).

[4] T. Hartmann, M. Babilon, S. Kamerdzhiev, E. Litvinova, D. Savran, S. Volz, and A. Zilges, Phys. Rev. Lett. **93**, 192501 (2004).

[5] P. Adrich, A. Klimkiewicz, M. Fallot, K. Boretzky, T. Aumann, D. Cortina-Gil, *et al.*, Phys. Rev. Lett. **95**, 132501 (2005).

[6] D. Savran, M. Fritzsche, J. Hasper, K. Lindenberg, S. Müller, V. Yu. Ponomarev, K. Sonnabend, A. Zilges, Phys. Rev. Lett. **100**, 232501 (2008).

[7] R. Schwengner, G. Rusev, N. Tsoneva, N. Benouaret, R. Beyer, M. Erhard, *et al.*, Phys. Rev. **C** 78, 064314 (2008).

[8] O. Wieland, A. Bracco, F. Camera, G. Benzoni, N. Blasi, S. Brambilla, *et al.*, Phys. Rev. Lett. **102**, 092502 (2009).

[9] A.P. Tonchev, S.L. Hammond, J.H. Kelley, E. Kwan, H. Lenske, G. Rusev, W. Tornow, and N. Tsoneva, Phys. Rev. Lett. **104**, 072501 (2010).

[10] R. Schwengner, R. Massarczyk, G. Rusev, N. Tsoneva, D. Bemmerer, R. Beyer, *et al.*, Phys. Rev. C **87**, 024306 (2013).

[11] A.P. Tonchev, N. Tsoneva, C. Bhatia, C.W. Arnold, S. Goriely, S.L. Hammond, J.H. Kelley, E. Kwan, H. Lenske, J. Piekarewicz, R. Raut, G. Rusev, T. Shizuma, and W. Tornow, Phys. Lett. B **773**, 20 (2017).

[12] M. N. Harakeh and A. van der Woude, *'Giant Resonances: fundamental high-frequency modes of nuclear excitation'*, Clarendon Press, Oxford, (2001).

[13] N. Paar, D. Vretenar, E. Khan, and G. Colò, Rep. Prog. Phys. **70**, 691 (2007).

[14] N. Tsoneva, H. Lenske, and Ch. Stoyanov, Phys. Lett. B **586**, 213 (2004).

[15] N. Tsoneva and H. Lenske, Phys. Lett. B **695**, 174(2011).

[16] N. Tsoneva and H. Lenske, Phys. Rev. C **77**, 024321 (2008).

[17] N. Tsoneva and H. Lenske, Physics of Atomic Nuclei **79**, 885 (2016).

[18] J. Piekarewicz, Phys. Rev. C **73**, 044325 (2006).

[19] J. Piekarewicz, Phys. Rev. C **83**, 034319 (2011).

[20] T. Inakura and H. Nakada, Phys. Rev. C **92**, 064302 (2015).

[21] X. Roca-Maza, *et al.*, Phys. Rev. C **92**, 064304 (2015).

[22] A. Brown, Phys. Rev. Lett. **85**, 5296 (2000).

[23] C. J. Horowitz and J. Piekarewicz, Phys. Rev. Lett. **86**, 5647 (20001).

[24] R. Raut, A. P. Tonchev, G. Rusev, W. Tornow, C. Iliadis, M. Lugaro, J. Buntain, S. Goriely, J. H. Kelley, R. Schwengner, A. Banu, and N. Tsoneva, Phys. Rev. Lett. **111**, 112501 (2013).

[25] N. Tsoneva, S. Goriely, H. Lenske, and R. Schwengner, Phys. Rev. C **91**, 044328 (2015).

[26] J. Enders, P. von Brentano, J. Eberth, A. Fitzler, C. Fransen, R.-D. Herzberg, H. Kaiser, L. Käubler, P. von Neumann-Cosel, N. Pietralla, V.Yu. Ponomarev, A. Richter, R. Schwengner, and I. Wiedenhöver, Nucl. Phys. A **724**, 243 (2003).
J. Enders, P. von Brentano, J. Eberth, A. Fitzler, C. Fransen, R.-D. Herzberg, H. Kaiser, L. Käubler, P. von Neumann-Cosel, N. Pietralla, V.Yu. Ponomarev, H. Prade, A. Richter, H. Schnare, R. Schwengner, S. Skoda, H.G. Thomas, T. Tiesler, D. Weisshaar, and I. Wiedenhöver,

[27] R. Schwengner, R. Beyer, F. Dönau, E. Grosse, A. Hartmann, A.R. Junghans, S. Mallion, G. Rusev, K. D. Schilling, W. Schulze, and A. Wagner, Nucl. Instrum. Methods A **555**, 211 (2005).

[28] R. Schwengner, G. Rusev, N. Benouaret, R. Beyer, M. Erhard, E. Grosse, A. R. Junghans, J. Klug, K. Kosev, L. Kostov, C. Nair, N. Nankov, K. D. Schilling, and A. Wagner, Phys. Rev. C **76**, 034321 (2007).

[29] G. Rusev, R. Schwengner, F. Dönau, M. Erhard, E. Grosse, A. R. Junghans, K. Kosev, K. D. Schilling, A. Wagner, F. Bečvář, and M. Krtička, Phys. Rev. C **77**, 064321 (2008).

[30] U. Kneissl, H. H. Pitz, and A. Zilges, Prog. Part. Nucl. Phys. **37**, 349 (1996); U. Kneissl, N. Pietralla, and A. Zilges, J. Phys. G **32**, R217 (2006).

[31] J. H. Kelley, E. Kwan, J.E. Purcell, C. G. Sheu, and H. R. Weller, Nucl. Phys. A **880**, 88 (2012).

[32] F. Metzger, in *Progress in Nuclear Physics*, edited by O. Frisch(Pergamon Press, New York, 1959), Vol. 7, pp. 53-88.

[33] S. Agostinelli *et al.*, Nucl. Instrum. Methods A **506**, 250 (2003).

[34] E. Haug, Radiat. Phys. Chem. **77**, 207 (2008).

[35] G. Roche, C. Ducos, and J. Proriol, Phys. Rev. A **5**, 2403 (1972).

[36] F. Salvat, J.D. Martinez, R. Mayol, and J. Parellada, Phys. Rev. A **36**, 467 (1987).

[37] G. Rusev, A.P. Tonchev, R. Schwengner, C. Sun, W. Tornow, and Y. K. Wu, Phys. Rev. C **79**, 047601 (2009).

[38] R. Jenkins, R. W. Gould, and D. Gedke, *Quantitative X-ray Spectroscopy* (Dekker, New York, 1995).

[39] E. Kwan, G. Rusev, A. S. Adekola, F. Dönau, S. L. Hammond, C. R. Howell, H. J. Karwowski, J. H. Kelley, R. S. Pedroni, R. Raut, A.P. Tonchev, and W. Tornow Phys. Rev. C **83**, 041601(R) (2011).

[40] R. Schwengner, R. Massarczyk, R. Beyer, M. Bhike, B. A. Brown, Krishichayan, K. Sieja, W. Tornow, D. Bemmerer, M. Butterling, V. Derya, M. Dietz, F. Fiedler, U. Friman-Gayer, A. Frotscher, M. Grieger, A. Hartmann, A. R. Junghans, T. Kögler, F. Ludwig, B. Lutz, H. Pai, T. Szücs, M. P. Takács, and A. Wagner, Phys. Rev. C **101**, 064303 (2020).

[41] T. Shizuma, T. Hayakawa, H. Ohgaki, H. Toyokawa, T. Komatsubara, N. Kikuzawa, A. Tamii, and H. Nakada, Phys. Rev. C **78**, 061303(R) (2008).

[42] T. Shizuma, N. Iwamoto, A. Makinaga, R. Massarczyk, R. Schwengner, R. Beyer, D. Bemmerer, M. Dietz, A. Junghans, T. K´ogler, F. Ludwig, S. Reinicke, S. Schulz, S. Urlaß, and A. Wagner Phys. Rev. C **98**, 064317 (2018).

[43] T. Shizuma, F. Minato, M. Omer, T. Hayakawa, H. Ohgaki, and S. Miyamoto, Phys. Rev. C **103**, 024309 (2021).

[44] V. G. Soloviev, *Theory of complex nuclei* (Oxford: Perg-

amon Press, 1976).
[45] V. Yu. Ponomarev, Ch. Stoyanov, N. Tsoneva, and M. Grinberg, Nucl. Phys. A **635**, 470 (1998).
[46] M. Grinberg and Ch. Stoyanov, Nucl. Phys. A **573**, 231 (1994).
[47] M. Spieker, A. Heusler, B. A. Brown, T. Faestermann, R. Hertenberger, G. Potel, M. Scheck, N. Tsoneva, M. Weinert, H.-F. Wirth, and A. Zilges, Phys. Rev. Lett. **125**, 102503 (2020).
[48] M. Weinert, M. Spieker, G. Potel, N. Tsoneva, M. M 端 scher, J. Wilhelmy, and A. Zilges, Phys. Rev. Lett. **127**, 242501 (2021).

TABLE I: Results of the ^{206}Pb(γ,γ') measurements. The excitation energies E_x, the angular distribution ratios $W(90°)/W(127°)$, the spin assignments J, the ratios Γ_0^2/Γ, and the branching ratios Γ_0/Γ are given. The values of Γ_0^2/Γ known from previous measurements are also listed for comparison.

E_x[∗] (keV)	$W(90°)/W(127°)$	J	Γ_0^2/Γ[†] (eV)	Γ_0/Γ	Γ_0^2/Γ[‡] (eV)
3656.5(1)	0.80(11)	1	0.194(16)	1.0	0.12(1)
3892.7(5)	1.2(4)	1	0.071(14)	1.0	0.03(1)
4379.6(2)	2.44(29)	2	0.149(16)	1.0	0.11(1)
4413.9(3)	2.2(4)	2	0.099(14)	1.0	
4596.3(3)	0.84(15)	1	0.111(12)	1.0	0.09(2)
4804.0(4)	0.59(14)	1	0.100(12)	1.0	
4860.4(3)	1.10(19)	1	0.099(11)	1.0	
4922.5(2)	0.62(10)	1	0.36(4)	1.0	0.18(4)
4932.6(3)	0.68(18)	1	0.180(23)	1.0	0.09(4)
4948.4(6)	0.80(28)	1	0.121(25)	1.0	
4960.3(2)	0.68(17)	1	0.178(21)	1.0	
4979.9(1)	0.75(5)	1	1.00(7)	1.0	0.79(26)
5011.8(1)	0.77(7)	1	0.87(6)	1.0	0.54(6)
5059.4(3)	0.83(21)	1	0.085(15)	1.0	
5206.9(2)	0.82(13)	1	0.246(24)	1.0	
5224.9(4)	0.72(17)	1	0.114(24)	1.0	
5282.7(2)	0.70(14)	1	0.222(24)	1.0	0.16(12)
5316.0(3)	0.76(16)	1	0.125(21)	1.0	
5358.9(5)	1.1(3)	1	0.063(17)	1.0	
5365.8(6)	0.88(25)	1	0.049(18)	1.0	0.08(6)
5398.1(3)	0.69(15)	1	0.234(26)	1.0	0.16(4)
5431.9(6)	0.65(17)	1	0.24(3)	1.0	
5464.7(4)	0.56(16)	1	0.38(4)	1.0	
5601.2(3)	1.06(22)	1	0.184(24)	1.0	
5635.5(3)	1.1(4)	1	0.060(18)	1.0	
5674.2(3)	0.86(17)	1	0.212(27)	1.0	0.22(4)
5694.7(4)	1.01(25)	1	0.161(25)	1.0	
5734.0(1)	0.72(5)	1	1.24(9)	1.0	
5776.3(2)	0.90(8)	1	0.73(5)	1.0	0.91(13)
5792.4(4)	0.78(20)	1	0.27(4)	1.0	0.33(7)
5812.3(3)	0.83(18)	1	0.25(3)	1.0	0.17(14)
5827.5(1)	0.76(8)	1	0.80(6)	1.0	0.8(10)
5837.0(2)	0.80(17)	1	0.28(4)	1.0	0.37(6)
5852.6(4)	1.0(4)	1	0.172(22)	1.0	
5878.1(2)	0.76(12)	1	0.26(3)	1.0	0.28(6)
5890.1(1)	0.77(10)	1	0.38(4)	1.0	0.35(6)
5908.8(3)	0.83(17)	1	0.25(3)	1.0	
5918.4(5)	1.03(27)	1	0.122(18)	1.0	
5940.4(1)	0.76(6)	1	0.94(7)	0.84(4)	0.82(30)
5966.9(1)	0.75(8)	1	0.61(5)	1.0	0.58(8)
5980.3(1)	0.77(7)	1	0.99(8)	1.0	1.11(14)
5995.9(7)	0.62(23)	1	0.16(4)	1.0	0.18(12)
6008.9(3)	0.75(14)	1	0.35(4)	1.0	0.32(6)
6019.4(3)	0.86(13)	1	0.231(24)	1.0	0.46(23)
6055.9(2)	0.93(10)	1	0.241(21)	1.0	0.24(7)
6064.9(3)	0.81(12)	1	0.270(28)	1.0	0.31(8)
6078.8(6)	0.90(19)	1	0.176(29)	1.0	0.28(8)
6084.1(4)	0.83(15)	1	0.217(29)	1.0	0.30(8)
6108.2(3)	1.10(14)	1	0.47(5)	1.0	0.20(14)
6147.9(3)	0.98(12)	1	0.57(5)	1.0	0.49(12)
6159.1(5)	0.50(9)	1	0.43(5)	0.65(9)	0.43(12)
6193.8(3)	0.8(3)	1	0.062(20)	1.0	0.27(16)
6211.0(3)	0.87(16)	1	0.21(3)	1.0	0.28(17)
6229.1(3)[§]	1.1(3)	1	0.144(25)	1.0	0.32(9)
6252.7(2)	0.62(15)	1	0.23(3)	1.0	0.46(10)

6276.1(4)	1.04(21)	1	0.114(16)	1.0	0.35(11)
6293.3(4)	0.77(15)	1	0.143(17)	1.0	
6308.0(2)	0.74(10)	1	0.41(4)	1.0	
6322.8(2)	1.01(13)	1	0.38(4)	1.0	0.96(23)
6360.4(3)	0.57(11)	1	0.22(3)	1.0	
6410.2(2)	0.86(9)	1	0.328(27)	1.0	0.48(21)
6456.8(2)	0.83(10)	1	0.31(4)	1.0	0.41(17)
6468.1(4)[¶]	0.68(12)	1	0.24(3)	1.0	0.38(20)
6492.5(3)	1.05(14)	1	0.202(21)	1.0	
6501.9(2)	0.75(9)	1	0.274(25)	1.0	
6546.4(3)	0.91(12)	1	0.215(22)	1.0	
6568.5(3)	1.04(13)	1	0.189(21)	1.0	
6627.9(1)	0.81(10)	1	0.54(5)	1.0	
6681.9(2)	0.83(10)	1	0.63(5)	1.0	
6705.8(3)	0.79(11)	1	0.37(3)	1.0	
6721.4(1)	0.81(7)	1	1.16(9)	1.0	
6765.0(3)	0.70(12)	1	0.65(7)	1.0	
6793.8(4)	1.13(26)	1	0.16(4)	1.0	
6820.4(3)	0.70(12)	1	0.52(6)	1.0	
6851.3(3)	0.88(16)	1	0.36(5)	1.0	
6872.9(4)	0.53(20)	1	0.24(4)	1.0	
6900.6(3)	0.76(10)	1	0.36(4)	1.0	
6911.6(5)	0.94(18)	1	0.201(29)	1.0	
6969.1(2)	0.73(6)	1	0.91(8)	0.63(4)	
6991.8(5)	0.8(4)	1	0.11(3)	1.0	
7013.3(2)	0.85(8)	1	0.52(4)	1.0	
7025.2(2)	0.74(6)	1	0.87(6)	1.0	
7038.8(4)	0.76(13)	1	0.229(28)	1.0	
7064.2(4)	1.02(12)	1	0.33(3)	1.0	
7079.3(3)	1.03(10)	1	0.44(4)	1.0	
7097.9(3)	0.67(10)	1	0.35(3)	1.0	
7118.5(1)	0.75(5)	1	1.23(9)	1.0	
7128.7(2)	0.78(7)	1	0.78(6)	1.0[**]	
7141.0(3)	0.71(9)	1	0.42(4)	1.0	
7155.1(4)	0.54(10)	1	0.31(3)	1.0	
7223.5(3)	0.90(8)	1	0.67(5)	1.0	
7233.7(3)	1.05(10)	1	0.57(5)	1.0	
7270.3(2)	0.91(7)	1	0.99(8)	1.0	
7279.7(1)	0.81(5)	1	2.78(19)	0.90(3)	
7304.1(2)	0.81(7)	1	0.77(6)	1.0	
7327.3(2)	0.89(7)	1	0.93(7)	1.0	
7353.8(4)	0.95(12)	1	0.33(3)	1.0	
7367.7(5)	0.91(14)	1	0.29(3)	1.0[††]	
7398.4(2)	0.86(7)	1	0.90(7)	1.0	
7409.8(5)	1.18(15)	1	0.31(3)	1.0	
7430.2(2)	0.87(7)	1	0.79(6)	0.60(3)	
7455.2(3)	0.87(8)	1	0.59(5)	1.0	
7535.6(2)	0.72(6)	1	0.93(7)	1.0	
7551.6(3)	0.68(9)	1	0.47(4)	0.34(3)	
7569.3(3)	0.63(8)	1	0.51(4)	1.0	
7660.1(4)	0.64(11)	1	0.34(4)	1.0	
7679.2(5)	0.72(13)	1	0.30(4)	0.36(5)	
7706.8(3)	0.86(9)	1	0.60(5)	1.0	
7721.4(2)	0.60(6)	1	0.71(6)	1.0	
7743.3(3)	0.59(8)	1	0.50(4)	1.0	
7760.9(4)	0.64(9)	1	0.42(4)	0.65(7)	
7778.0(2)	0.69(6)	1	0.93(7)	1.0	
7794.7(5)	0.85(14)	1	0.27(3)	1.0	
7830.5(4)	0.67(9)	1	0.34(3)	1.0	
7841.0(5)	0.83(11)	1	0.40(4)	0.51(5)	
7853.0(5)	0.68(11)	1	0.32(4)	1.0	
7883.0(5)	0.63(11)	1	0.33(4)	1.0	
7894.8(7)	0.84(17)	1	0.23(3)	1.0	
7909.4(4)	0.63(9)	1	0.40(4)	1.0	

7951.5(3)	0.78(9)	1	0.52(5)	0.44(3)
7970.6(4)	0.98(13)	1	0.35(4)	1.0
7988.9(4)	0.63(10)	1	0.37(4)	1.0
8033.2(4)	0.80(11)	1	0.34(4)	1.0
8060.8(3)	0.94(10)	1	0.47(4)	1.0
8087.6(3)	0.70(7)	1	0.61(5)	0.31(2)
8113.0(5)	0.50(9)	1	0.32(3)	1.0
8125.4(4)	0.59(9)	1	0.39(4)	1.0
8145.7(4)	0.48(9)	1	0.35(4)	1.0
8161.0(3)	0.77(9)	1	0.51(4)	1.0
8177.1(5)	0.50(10)	1	0.34(4)	1.0
8189.1(4)	0.66(9)	1	0.40(4)	1.0
8255.5(4)	0.73(12)	1	0.32(3)	1.0
8277.0(4)	0.53(8)	1	0.42(4)	1.0
8304.0(3)	0.79(9)	1	0.49(4)	1.0
8316.6(4)	0.78(9)	1	0.54(5)	1.0
8327.3(7)	0.90(16)	1	0.24(3)	1.0

[a]The peak fitting error in parenthesis is given in units of the last digit. This energy was deduced from the γ-ray energy measured at 127° to the beam.

[b]This work. The statistical and systematic uncertainties(associated with strength normalization, photon flux, and efficiency) are reflected in the errors.

[c]Values taken from [26].

[d]This transition is known from previous work [26] and coincides with a possible branch of the state at 7129 keV.

[e]This transition is known from previous work [26] and coincides with a possible branch of the state at 7368 keV.

[f]Possible branch to the 2_1^+ state coincides with the transition at 6229 keV.

[g]Possible branch to the 2_1^+ state coincides with the transition at 6468 keV.